Journal of Colloid and Interface Science 504 (2017) 669–679

Contents lists available at ScienceDirect

Journal of Colloid and Interface Science

journal homepage: www.elsevier.com/locate/jcis

Regular Article

Kinetic and isotherm studies on adsorption of toxic pollutants using porous ZnO@SiO_2 monolith

Manisha Sharma [a], Satyajit Hazra [b], Soumen Basu [a,*]

[a] School of Chemistry and Biochemistry, Thapar University, Patiala, Punjab 147004, India
[b] Saha Institute of Nuclear Physics, Kolkata 700064, India

GRAPHICAL ABSTRACT

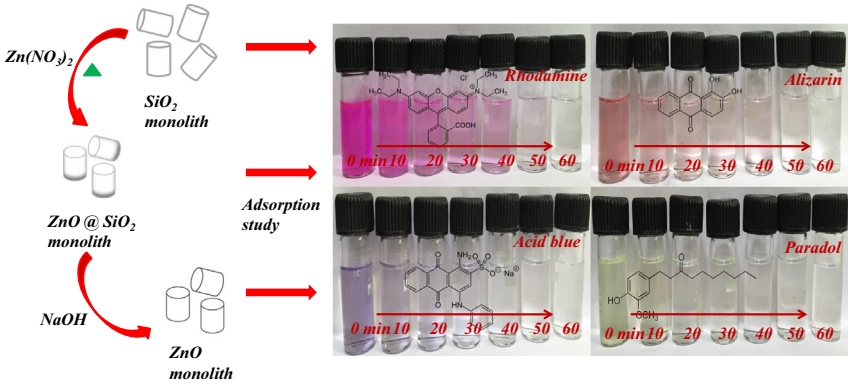

ARTICLE INFO

Article history:
Received 3 April 2017
Revised 29 May 2017
Accepted 6 June 2017
Available online 7 June 2017

Keywords:
ZnO monolith
Adsorption
Pesticide
Dyes
Isotherm and kinetics

ABSTRACT

Removal of toxic effluents (like dyes and pesticides) by cost-effective and user-friendly method is needed to provide sustaining the environment for civilization. Here, low-cost mesoporous silica monolith (SiO_2) and silica supported metal-oxide (ZnO@SiO_2) monolith were synthesized to reduce the solemn impact of toxic effluents. Batch experiments were performed to remove Alizarin (AZ), Paradol (PD), Acid blue-113 (AB) and Rhodamine-B (RD) from aqueous solution via synthesized monoliths. The influence of various parameters (like pH, contact time, temperature and adsorbate concentration) has been optimized. The maximum adsorption capacity of ZnO@SiO_2 monolith is 625, 500, 714 and 555 mg/g for AZ, RD, AB, and PD respectively. The adsorption for AZ, PD, AB, and RD is spontaneous and exothermic. The adsorption process can be well described by the pseudo-second-order kinetic model (high regression coefficients) and the Freundlich isotherm model (R^2 = 0.97–0.99).

1. Introduction

In the recent era, water resources get polluted due to growth in population and industrial activities. Ground water and surface water gets contaminated by the excess release of toxic and some colored effluents like pesticides (substances used to destroy insects or pests) and organic dyes (unprocessed colored substances) [1]. These toxic wastes (agrochemical residues/organic pollutants) are highly hazardous to aquatic living, agriculture, animal and human health. Toxic effluents containing dyes and pesticides need to be treated before being delivered to the environment due to their toxic and carcinogenic effects on the living system including human beings by causing skin irritations, allergies, etc. [2–4].

* Corresponding author.
E-mail address: soumen.basu@thapar.edu (S. Basu).

http://dx.doi.org/10.1016/j.jcis.2017.06.020
0021-9797/

Among several physical or chemical methods, adsorption process can be used as a conventional method as it is utmost effective, cost effective, eco-friendly and easy to use. In this process, pollutants are transferred from aqueous medium onto the surface of the solid material. Also, adsorbents with high surface reactivity, surface area and with a high number of the vacant site are in demand. Several adsorbents (natural or synthetic) such as polymers, activated carbon, agro-industrial wastes, zeolite and CNTs [5–7] have been used as adsorbents for the treatment of contaminated water.

Porous material, mainly those with bimodal porosity, used as an essential material to numerous important application including heterogeneous catalysis, adsorption and separation process. Due to the presence of a high number of reactive sites, porous composites are considered as a novel adsorbent for pre-concentration of toxic effluents [8–10]. Recently, mesoporous metal oxides (like Al_2O_3, MgO, SnO_2, Fe_3O_4 and TiO_2) have gained huge attention for adsorption of organic pollutants because of their high surface area, reusability and more efficiency metal oxides other than ZnO have already been reported for toxic effluent removal [11,12]. In literature, nano ZnO (metal-oxide) have been used for remediation of pollutants in water. Nonetheless, most of the literature has been focused on the photocatalytic activity of ZnO and studies regarding adsorptive affinity of ZnO in the direction of pollutant removal are still insufficient. Because of non-toxicity, easy producibility, and high adsorptive properties, mesoporous ZnO composites are considered as one of the most competent adsorbents for the removal of various toxic pollutants [13–15]. With controllable porosity, surface area and high available adsorption sites of ZnO nanocomposites enhance its utility for various other applications, especially for removal or adsorption of toxic pollutants [16–18].

ZnO can be synthesized by different methods including hydrothermal, sol-gel, microwave irradiation, etc. Using nanocasting method, hierarchically porous ZnO monoliths of desired length scale can be synthesized. This process has already been used to prepare porous monoliths of carbon, NiO, TiO_2, Co_3O_4, SnO_2, MnO_2, ZrO_2, Al_2O_3, Cr_2O_3, In_2O_3, CeO_2, Fe_2O_3, Y_2O_3 and various mixed-oxides [19–25]. Ordered porous oxides because of their large surface areas, large pore volumes and ordered pore networks have a wide range of potential applications in energy storage, nanoreactors, semiconductors, electronic devices, catalysis and gas sensors [26]. Chitosan-polyaniline/ZnO hybrids were used as an adsorbent for removal of reactive orange-16 dye and the maximum adsorption efficiency was found 476.2 mg g^{-1} [27]. Removal of bromophenol red was investigated using ZnO nanoparticles loaded on activated carbon; maximum adsorption efficiency was found 200 mg g^{-1} [28]. Mostly, ZnO nanocomposites are available in powder form which has disadvantages since they make a miscible suspension with water. Therefore; the fast and economical method is needed for the growth of unsurpassed system for solid phase extraction from solution. So in this regard, we tried to make mesoporous silica supported ZnO monoliths (solid rock style material) for pesticide and dye adsorption, which is cost effective. However, up to date, the efficient removal of organic toxic pollutants using solid ZnO@SiO_2 monoliths has not been studied yet. In this work synthesis of mesoporous ZnO@SiO_2 monoliths via nanocasting process from hierarchically porous parental silica monolith has been discussed in detail. The efficient removal of pesticides and dyes using solid ZnO@SiO_2 monoliths has been studied in detail. The effect of several physicochemical parameters, such as sorbent particle size, pH, contact time and pollutant concentration as well as the thermodynamic parameters are calculated and discussed. The kinetic data are modeled by the pseudo-first-order, pseudo-second-order, and Elovich's models. The Langmuir and Freundlich models were used to describe equilibrium isotherms. Our results indicate that the high adsorption capacity for pesticide and dye solutions will promote the application of ZnO@SiO_2 monolith as advanced adsorbent materials.

2. Material and methods

All chemicals used are commercially available and used as received. Polyethylene glycol (PEG) (Molecular weight - 35,000 g/mol) and octadecyltrimethylammonium bromide (CTAB) were purchased from Sigma-Aldrich. Tetraethoxysilane (TEOS) were purchased from Alfa Aesar. Nitric acid (69%), ammonia (28–30%), zinc nitrate hexahydrate ($Zn(NO_3)_2{\cdot}6H_2O$), rhodamine-B, acid blue-113 and alizarine were purchased from Merck. Paradol was gifted by Anu products Ltd. Darya Ganj, Delhi, India.

2.1. Synthesis of SiO_2 monoliths

PEG (0.55 g) was added in 8.25 ml distilled water and stirred the solution at room temperature. Later, TEOS (8.1 ml) and 1.38 ml nitric acid (30%) were added to the above solution and mixed by stirring until a translucent sol was obtained. After that, 1.3 g CTAB was added to the sol with continuous stirring until it gets dissolved completely. Here, CTAB was used as surfactant template for the formation of mesoporous structures in monoliths. The obtained sol was transferred to microplates and 8–12 h time was required for sol to gel formation at 40 °C. Thereafter aging of the gel was done at 40 °C for 72 h. The solvent exchange was performed using NH_4OH (1 M) for 9 h at 90 °C, to increase the stability and the degree of condensation of the SiO_2 monoliths. Afterward, HNO_3 (0.1 M) solution was used to acidify SiO_2 monoliths. Synthesized monoliths were washed thoroughly with de-ionized water and were kept in an oven at 40 °C for 4–5 days for proper drying. Finally, freshly prepared monoliths were calcined at 550 °C for 5 h using 1 °C/min heating ramp.

2.2. Synthesis of ZnO@SiO_2 monoliths

ZnO@SiO_2 monoliths were synthesized via nanocasting method. Zinc nitrate hexahydrate (3.1 M) solution was impregnated into as prepared silica monoliths after degassing them under vacuum. The wet monoliths were heated at 150 °C for 10 h (1 °C/min). Impregnation process was repeated for at least five times to get uniform ZnO@SiO_2 monoliths. Later, synthesized composites were calcined at 400 °C for 5 h at a rate of 1 °C/min.

2.3. Characterization

The pH was adjusted and measured using a pH meter, model cyber scan pH 1100 (Eutech, Singapore). The absorbance of each pollutant was measured using a Champion UV-500 spectrophotometer. X-ray diffraction analysis (XRD) was done at room temperature using Pan Analytical (X'Pert-Pro) diffractometer using Cu Kα radiation (λ = 1.5406 Å) above a scanning interval (2θ) from 10° to 70°. The sample morphology and elemental analysis were studied by FESEM and EDS by Hitachi SU 8010 field emission scanning electron microscope operating at 30 kV. Surface area was evaluated through Brunauer–Emmett–Teller (BET) method and pore-size distributions were evaluated according to the Barrett–Joyner–Halenda (BJH) model by using BELSORP MINI-II (Bel, Japan) surface area and pore size analyzer. Before each set of measurements, samples were degassed at 200 °C in vacuum for more than 3 h.

2.4. Adsorption study

All the dyes (AZ, AB and RD) and pesticide (PD) adsorption on porous monoliths were executed in a batch system at room temperature using favorable conditions. Monoliths (0.02 g) were added into 100 ml of aqueous solution of dyes and pesticide (10–100 mg L^{-1}) and stirred for different time periods at a speed of 200 rpm. After the completion of adsorption, the solution was centrifuged for 10 min at 6000 rpm. After centrifugation, small amounts of the liquid were taken to be analyzed by UV–Vis absorption spectroscopy by monitoring the absorbance changes at λ_{max} 550 nm for AZ and RD, 565 nm for AB and 400 nm for PD. Chemical structure of different pollutants are shown in Fig. 1. The adsorption capacity (q_e) was calculated by the uptake amount of pollutants adsorbed per mass unit of metal oxide (mg/g) using the formula:

$$q_e = \frac{(C_o - C_e)}{m} \times V \quad (1)$$

while, C_0 is the initial and C_e is the equilibrium concentrations (mg/L), while V is the volume of the solution (L) and m is the weight of the adsorbent (g).

3. Results and discussion

Bimodal interconnected porous structures were obtained via phase separation and gelation after successively completing interaction between gelling silica/CTAB micelles and water soluble polymer (PEG). Fig. 2a shows the type IV, nitrogen sorption plot for SiO_2 and ZnO@SiO_2 monoliths which confirm the characteristics of mesoporous material. The characteristic parameters such as specific surface area, total pore volume and pore diameter of the synthesized monoliths are discussed in Table 1. The BJH pore size distribution indicates that the samples have pores in the range of 5–20 nm (Fig. 2b), which indicate the mesoporous nature of the materials.

The phase and purity of the synthesized ZnO@SiO_2 monoliths were confirmed by XRD analysis (Fig. 3a). XRD pattern confirms the formation of hexagonal structure of ZnO on the surface of SiO_2 monolith. ZnO@SiO_2 monolith shows dominant peaks for ZnO, 2θ at 31.8°, 34.4°, 36.23, 47.5, 56.6 and 62.8° corresponding to lattice planes of (100), (002), (101), (102), (110) and (103) respectively, which is confirmed by JCPDS card no. 36-1451 [29]. Inset of Fig. 3a shows mesoporous nature of SiO_2 monoliths. No other diffraction peaks corresponding to $Zn(NO)_2{\cdot}6H_2O$ and Zn $(OH)_2$ or other impurities have been found in the samples, indicating that the precursor has completely transformed into ZnO. Diffused reflectance spectra (DRS) or absorbance as a function of wavelength shows exciton absorption edges at 346 nm for ZnO (Fig. 3c) and its optical band gap (E_g) was calculated using the following equation:

$$(\alpha h\nu)^2 = A(h\nu - E_g)^n \quad (2)$$

where α is absorption coefficient, E_g represents optical band gap, A is a characteristic constant and hν is photon energy. The band gap of ZnO@SiO_2 monolith was evaluated according to intercept of the line obtained from Tauc plot (Fig. 3d). The presence of a single slope in the plot shows that the mesoporous monoliths have direct and allowed transitions. The optical band gap energy is obtained by extrapolating the straight line portion of the plot to zero absorption coefficient. The band gap value of ZnO was found to be 3.11 eV. FESEM images of the SiO_2 and ZnO@SiO_2 monoliths are shown in Fig. 4. The morphology of the macropores is very similar in both the cases. There appears to be fine mesopore structure within the walls of the macropores. The elemental composition of the synthesized monoliths was confirmed by EDS analysis (Fig. 4). Uniform distribution of the precursors throughout the core of the SiO_2 monoliths was responsible for chemical homogeneity.

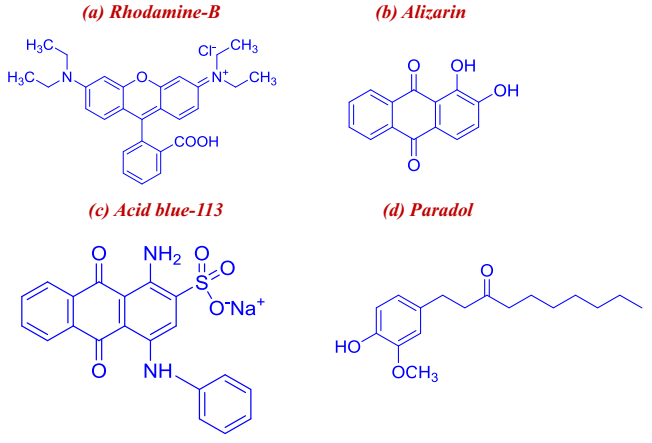

Fig. 1. Chemical structure of different pollutants.

3.1. Adsorption studies

3.1.1. Effect of pH

Adsorption of dyes and pesticide in the pores of monoliths depends on the pH of the solution, due to different degree of ionization, surface binding sites of adsorbents. Adsorption of pollutants by different monolith was studied at a pH range from 3 to 10. pH values were adjusted by addition of either NaOH or HNO_3 on the synthetic solution of pollutants [30–32]. Fig. 5a and b shows plots for the effect of pH on pollutant adsorption efficiencies of SiO_2 and ZnO@SiO_2 monolith. It was observed that the adsorption percentage increases with increase of pH (from pH 2 to 4). At pH 4, the adsorption process become highest, may be due to the maximum number of active sites present at the surface of adsorbent. Under the acidic conditions (at low pH), the surface of the adsorbents was surrounded by H^+ ions that interacts with anions of toxic pollutants. Higher adsorption for anionic dye (Acid blue), obtained at lower pH values may be due to electrostatic attraction between the negatively charged dye and positively charged adsorbent surface. Similarly for the cationic dye (Rhodamine B) the interaction is very less and as a result the % adsorption is decreases. For neutral dye (Alizarin) and pesticide (Paradol) the interaction is not effective and as a result the % adsorption is moderate.

3.1.2. Effect of contact time

The effect of contact time was analyzed between 10 and 60 min for the adsorption of pollutants by SiO_2 and ZnO@SiO_2 monoliths. A physical change can be observed in Fig. 5c and d. As the equilibrium time depends upon the initial concentration of pollutants, we have maintained the initial concentrations of the pollutants at 10 mg/L (pH 4). Pollutants were quantitatively adsorbed by the SiO_2 and ZnO@SiO_2 monoliths from the aqueous solution even after at a short time of exposure (<10 min). Since there was no significant increase in pollutants sorption after 40 min, the adsorption time of 60 min was kept for auxiliary experiments [33,34].

3.1.3. Effect of initial concentration of pollutants

Effect of the initial concentration of pollutants on the monolith (0.02 g) was studied by changing the initial pesticide and dyes concentrations in the range of 10–100 mg/L at most effective pH 4 and at room temperature (Fig. 5e and f). The initial concentration offers the desired driving forces to overcome the resistance to mass transfer of pollutant ions between aqueous and solid phase.

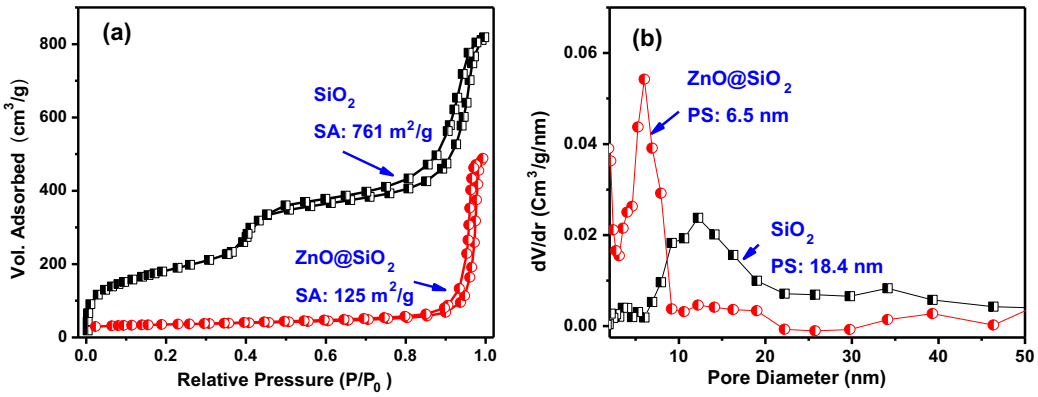

Fig. 2. (a) Nitrogen adsorption desorption curve, (b) Pore size distribution using BJH plot for SiO_2 and ZnO@SiO_2 monoliths.

Table 1
Textural characteristics for synthesized monoliths determined from nitrogen sorption measurements.

Monoliths	S_{BET} ($m^2\ g^{-1}$)	d (nm)	V_g ($cm^3\ g^{-1}$)
SiO_2	761	18.4	1.4
ZnO@SiO_2	125	6.5	0.3

Accordingly, increase in initial concentration also enhances the interaction between pollutants and monoliths. The results confirmed that the removal of pollutants was directly proportional to the initial concentrations of pollutants [35,36].

3.2. Adsorption kinetics

The kinetics of different pollutants adsorption on SiO_2 and ZnO@SiO_2 monoliths were also evaluated using pseudo-first-order rate equation and pseudo-second-order kinetic model [37,38]. The pseudo-first-order rate equation is usually used to predict adsorption kinetics and is expressed as;

$$\log(q_e - q_t) = \log(q_e) - \frac{K_1}{2.303}t \quad (3)$$

where q_e and q_t are a number of pollutants (mg/g) adsorbed at equilibrium and at any given time t (min) respectively and K_1 is the rate constant for the pseudo-first-order reaction for adsorption (min^{-1}). Activated adsorption can be defined by Elovich's equation. Also, this

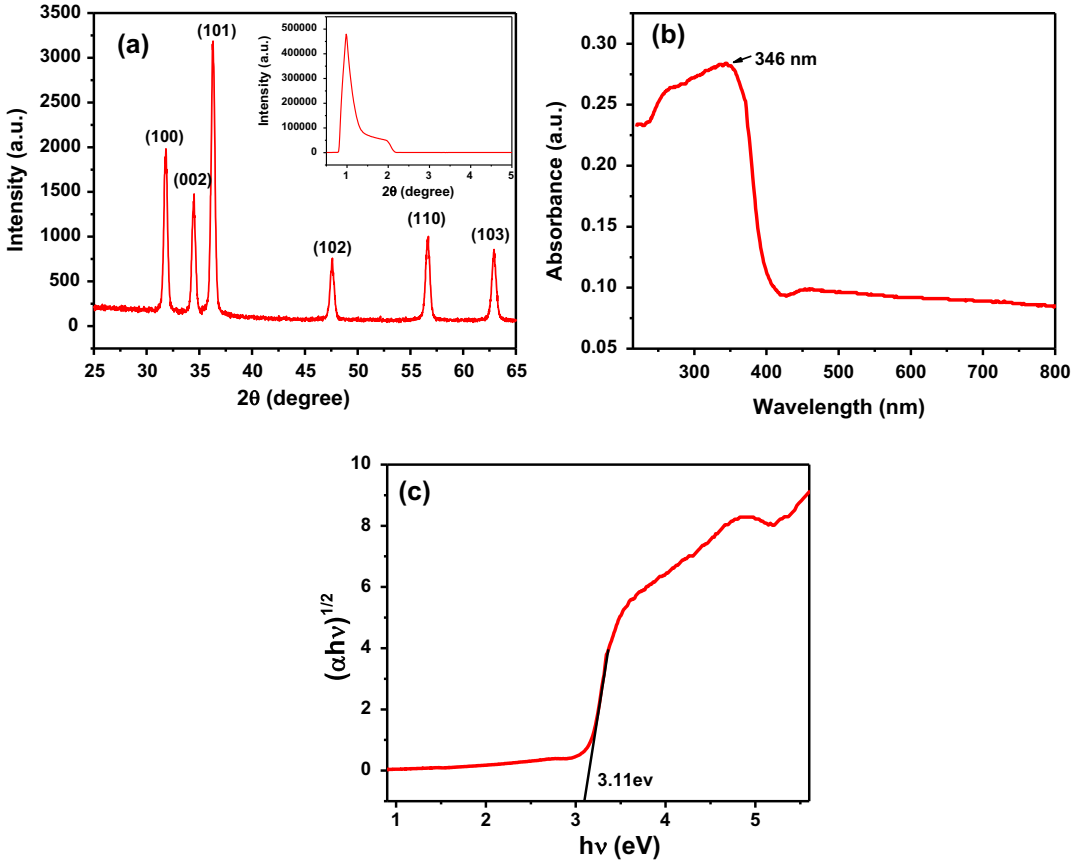

Fig. 3. (a) XRD pattern, (b) UV–vis spectrum and (c) Tauc plot for ZnO@SiO_2 monolith.

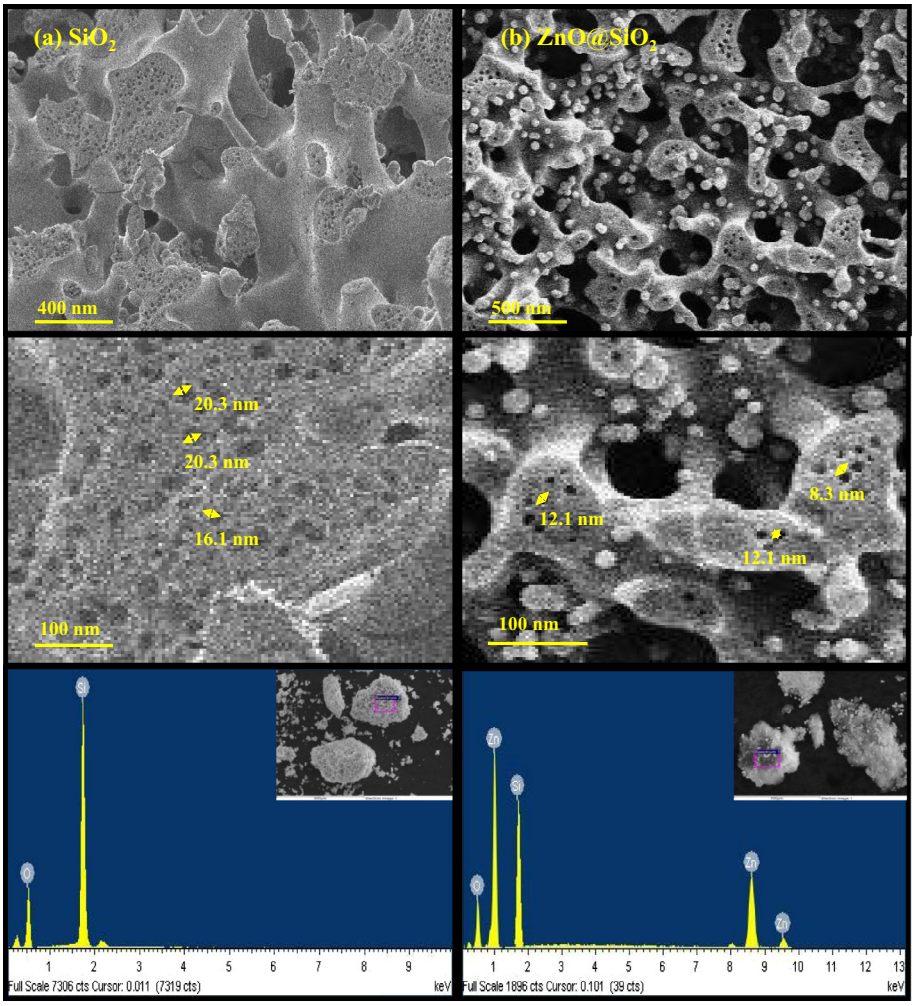

Fig. 4. FESEM and energy dispersive X-ray spectra for SiO_2 and ZnO@SiO_2 monoliths.

equation has been used for relating adsorption of pollutants from aqueous solution and can be expressed as;

$$q_t = \frac{1}{b}\ln(ab) + \frac{1}{b}\ln \quad (4)$$

where a and b are initial adsorption rate (mg/(g min)) and a desorption constant (g/mg) respectively. If this equation applies, it should lead to a straight line by plotting q_t as a function of ln(t) [39–41].

The pseudo-second-order rate equation is expressed as;

$$\frac{t}{q_t} = \frac{1}{k_2 q_e^2} + \frac{t}{q_e} \quad (5)$$

where q_e and q_t are a number of pollutants (mg/g) adsorbed at equilibrium and at any given time t (min) respectively and K_2 is the rate constant for pseudo-second order reaction for adsorption (g/mg min) [42]. Linear fit plots of pseudo-first-order, pseudo-second-order and Elovich's equation for synthesized monoliths for the adsorption of different pollutants are shown in Fig. 6. Table 2 shows the parameters obtained from the pseudo-first-order equation (q_e and K_1) of Elovich's equation (a and 1/b) and of the pseudo-second-order kinetic model (K_2 and q_e). However, correlation coefficients (R^2) were found near to unity for all batches. But, the sorption kinetics can be described more appropriately by a pseudo-second-order model than other kinetic models for all the investigated pollutants, as adsorption process was mostly controlled by chemisorption.

3.3. Adsorption isotherms

Adsorption isotherm gives proper quantitation of effectiveness of adsorption. The relationship between the concentrations of adsorbed and dissolved adsorbate at equilibrium along with the interactive behavior between the adsorbate and adsorbent can also describe by adsorption isotherm. In this study, Langmuir and Freundlich isotherm models were used to analyze the adsorption mechanisms, through which experimental results of pollutants can be explained in a wide range of concentrations. The Langmuir equation is expressed as follows;

$$\frac{C_e}{q_e} = \frac{1}{Q_o b} + \frac{C_e}{Q_o} \quad (6)$$

where, the adsorption capacity at equilibrium is q_e (mg/g) and the maximum amount of the AZ, AB, RD and PD adsorbed per unit weight of the adsorbent is Q_0 (mg/g). When the surface is entirely covered with pollutants, Q_0 represents the adsorption capacity, helping in the assessment of adsorption act of different adsorbents. Langmuir equilibrium constant (b) which is interrelated to the similarity of the connecting spots, shows the bond energy for the adsorption reaction. The linear plots of C_e/q_e vs. C_e propose the validity of the Langmuir isotherms and the values of Q_0 and b are obtained from slope and intercepts of the plots [43,44]. Plots for Langmuir isotherm for adsorption of different pollutants on monoliths are shown in Fig. 7a and b. The Freundlich isotherm is a resul-

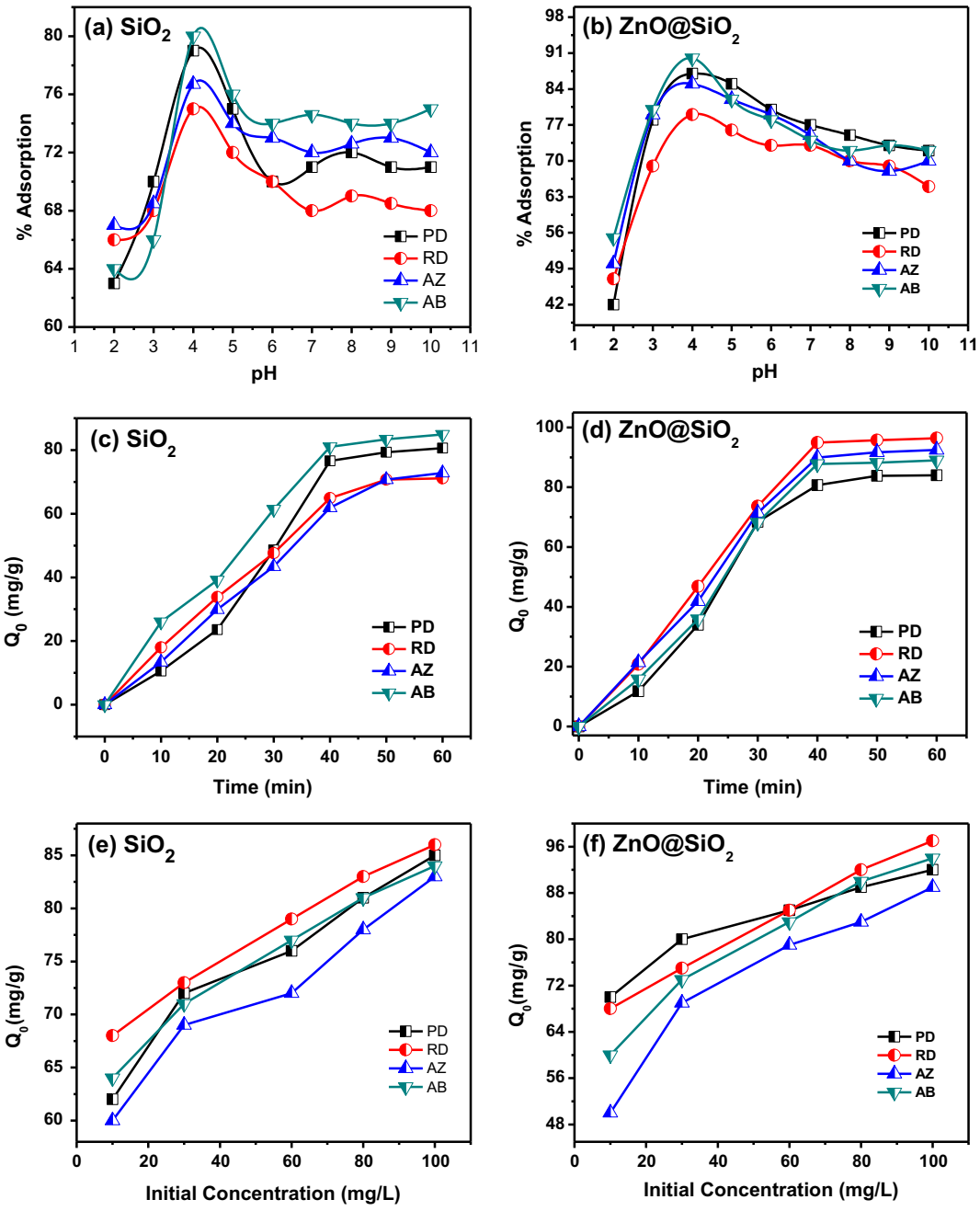

Fig. 5. Plot for (a and b) effect of pH, (c and d) effect of time and (e and f) effect of concentration for SiO_2 and ZnO@SiO_2 monoliths [concentration of monoliths: 0.02 g/L, speed of shaker: 200 rpm, temperature: 30 °C].

tant model of multilayer adsorption on the adsorbent. It can be described as:

$$\log q_e = \log K_f + \frac{\log C_e}{n} \tag{7}$$

Freundlich constants, K_f ($mg^{1-1/n}\,L^{1/n}\,g^{-1}$) and n, depict the adsorption capacity and intensity, respectively [45]. Freundlich isotherm plot for AZ, AB, RD and PD adsorption on different monoliths are shown in Fig. 7c and d. Isotherm parameters for Langmuir and Freundlich models are listed in Table 3.

Adsorption is considered as satisfactory when the Freundlich constant n takes values within the range (1–10). The higher the value of R^2 for Freundlich model indicating the better applicability of Freundlich model. A comparative maximum monolayer adsorption efficiency of different nanostructures for different pollutants is listed in Table 4 and here it could be concluded that the as-synthesized monoliths could be employed as an alternative adsorbent for toxic pollutants at low concentrations.

3.4. Intra-particle diffusion model

The adsorption kinetics may be defined from the mechanistic point of view occasionally and mechanism of adsorption can be evaluated by Weber-Morris model [51]. Generally, adsorption process involves either by one or more steps: surface diffusion, pore diffusion, film diffusion and adsorption on the pore surface, or a combination of more than one step. In a batch process, experimental sorption rate data relates the diffusive mass transfer by an

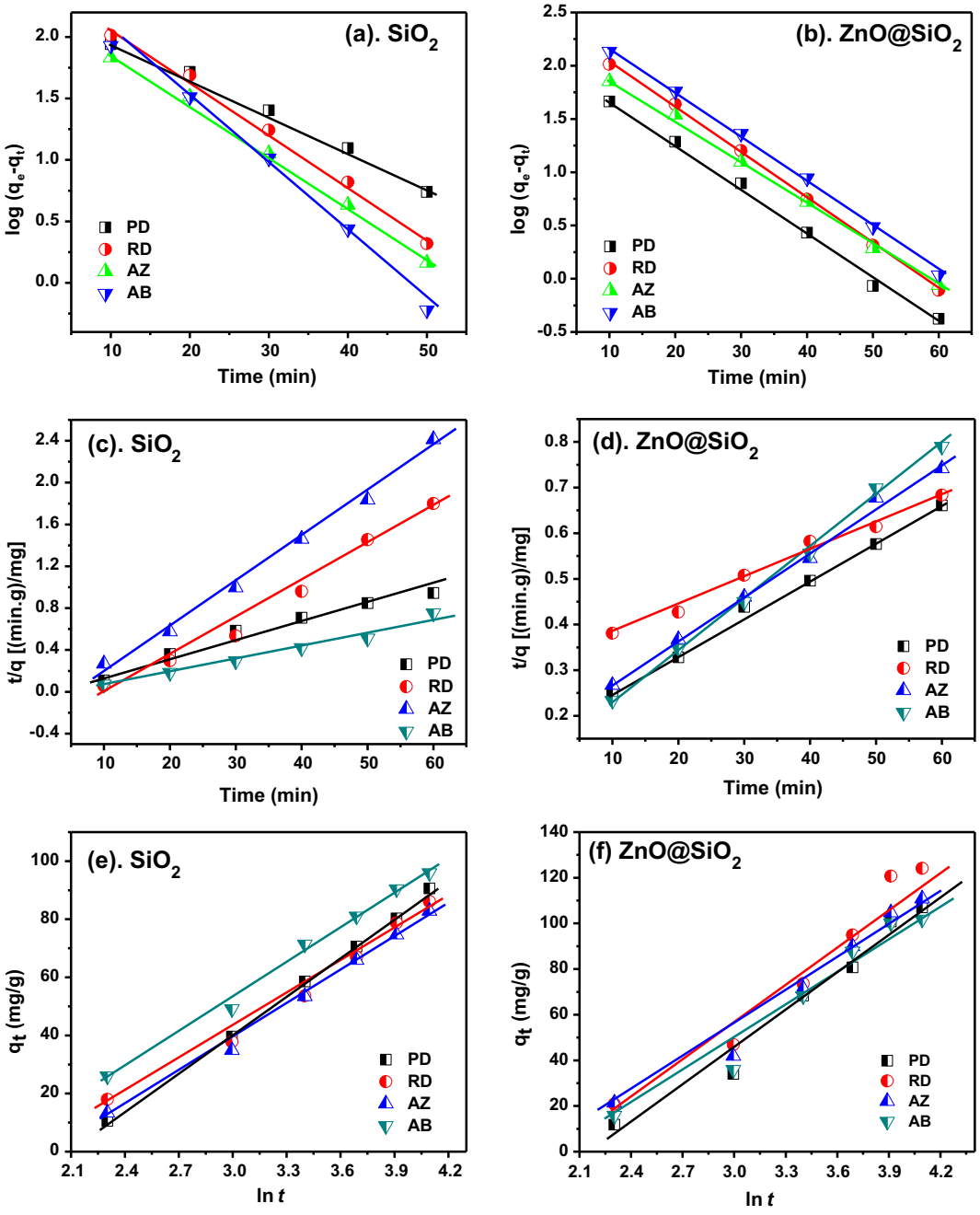

Fig. 6. Linear fit curves for (a and b) Pseudo first order, (c and d) Pseudo second order, (e and f) Elovich's model for SiO_2 and ZnO@SiO_2 monoliths [concentration of monoliths: 0.02 g/L, speed of shaker: 200 rpm, pH: 4, temperature: 30 °C].

Table 2
Kinetic parameters for adsorption of dyes and pesticide on different monoliths.

Adsorbent	Pollutants	Pseudo-first order			Elovich's equation			Pseudo-second order		
		q_e^*	$K_1 \times (10^{-2})^+$	R^2	$a^\$$	$1/b^*$	R^2	$K_2^@$	q_e^*	R^2
SiO_2	AZ	7.8	6.9	0.964	201.3	0.021	0.969	1.7×10^{-2}	32.5	0.990
	AB	9.6	9.6	0.985	291.3	0.024	0.953	3.4×10^{-2}	28.57	0.993
	RD	8.3	9.6	0.956	212.4	0.025	0.974	7.4×10^{-2}	23.8	0.983
	PD	10.7	12.2	0.880	265.5	0.026	0.936	0.18×10^{-2}	37.3	0.975
ZnO@ SiO_2	AZ	29.7	1.6	0.948	398.3	0.018	0.974	4.7×10^{-4}	111.1	0.995
	AB	33.6	1.86	0.960	431.9	0.018	0.977	10×10^{-4}	90.9	0.997
	RD	31.8	1.86	0.969	480.6	0.016	0.987	1.1×10^{-4}	166.6	0.999
	PD	28.2	1.8	0.986	477.6	0.017	0.949	3.7×10^{-4}	125	0.995

Where, * = mg/g; @ = g/(mg.min); $ = mg/(g.min); + = min^{-1}.

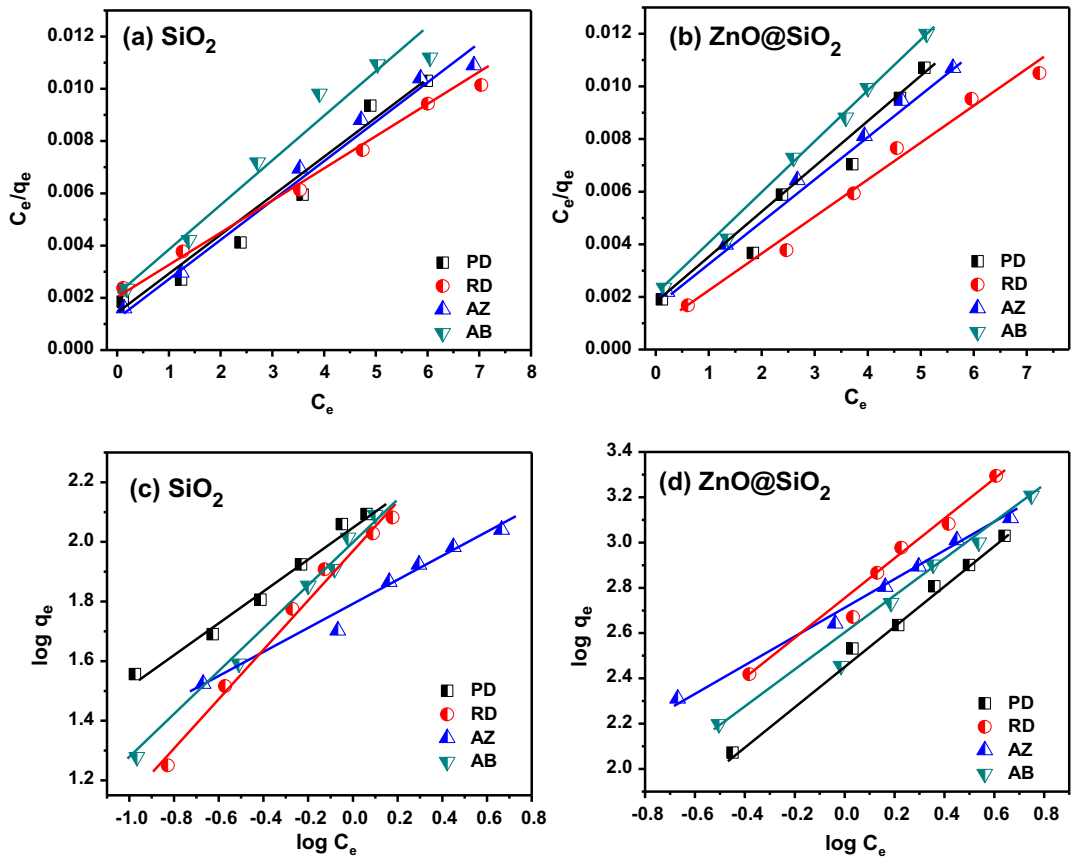

Fig. 7. Linear plots for isotherms (a and b) Langmuir and (c and d) Freundlich for SiO_2 and ZnO@SiO_2 monoliths [concentration of monoliths: 0.02 g/L, speed of shaker: 200 rpm, pH: 4, temperature: 30 °C].

Table 3
Comparison of isotherm parameters and coefficients for different pollutants over monoliths at room temperature.

Adsorbent	Pollutants	Langmuir			Freundlich		
		Q_0^+	B	R^2	K_f^{++}	n	R^2
SiO_2	AZ	102	0.05	0.991	4.8	1.1	0.997
	AB	123	0.14	0.979	6.9	1.5	0.996
	RD	83	0.04	0.966	6.9	1	0.980
	PD	96	0.19	0.990	7.3	1	0.999
ZnO@ SiO_2	AZ	625	0.84	0.987	14.9	1.62	0.993
	AB	714	1.05	0.896	12.9	1.20	0.978
	RD	500	2	0.986	15.1	1.16	0.994
	PD	556	1.5	0.966	11.8	1.14	0.996

Where, + = mg/g; ++ = $mg^{1-1/n}\,L^{1/n}\,g^{-1}$.

Table 4
A comparative account of the adsorption efficiency of different pollutants by different nanostructures.

Adsorbents	Surface area (m^2/g)	Pollutant	Maximum adsorption (mg/g)	Conditions	References
CPA/ZnO hybride	45.9	Orange 16 dye	476.2	Time-60 min	[27]
ZnO-NR-AC	–	Bromophenol red	200	pH-1–9 Time-24 min	[28]
Activated carbon	981	Pesticide (Methoxychlor)	112.0	pH-2 Temp-25 °C Time-60 min	[46]
ZnO nanoparticles	–	Victoria Blue	163.9	pH-2–10	[47]
ZnO/$ZnFe_2O_4$	94.4	Methylene Blue	37.27	pH-3–11	[29]
ZnO nanopowder	–	Reactive black	27.6	pH-3–9	[48]
MWCNTs	–	Alizarin red S	161.29	pH-1–6	[49]
Functionalized ZnO NPs		Brilliant blue R-250	59.9	pH-2–12	[50]
ZnO@SiO_2 monolith	110	Alizarin Acid Blue Rhodamine Paradol	625 714 500 555	pH-4, Time-80 min, Temp-25 °C	Present study

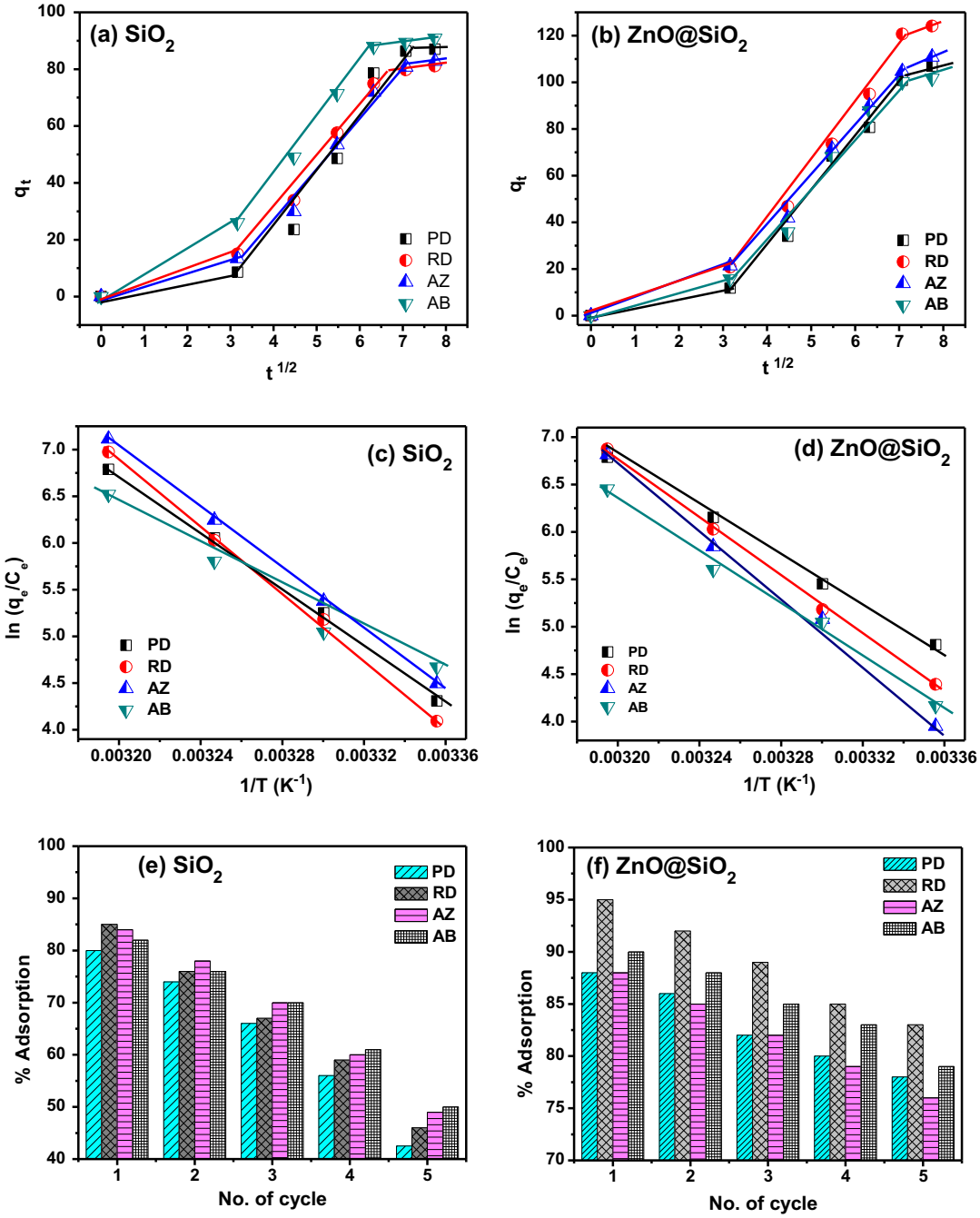

Fig. 8. Plot showing (a and b) Weber-Morris plot, (c and d) effect of temperature for adsorption studies on SiO_2 and ZnO@SiO_2 monoliths and (e and f) showing recyclability of monoliths [concentration of monoliths: 0.02 g/L, speed of shaker: 200 rpm, pH: 4, dye concentration: 10 mg/L].

Table 5
Intra-particle diffusion parameters for the adsorption of dyes and pesticide.

Adsorbent	Pollutants	K_i	I	R^2
SiO_2	AZ	0.16	2.1	0.862
	AB	0.16	2.9	0.923
	RD	0.15	3.3	0.890
	PD	0.19	2.6	0.935
ZnO@SiO_2	AZ	0.20	4.5	0.985
	AB	0.24	4.9	0.965
	RD	0.20	5.2	0.987
	PD	0.22	5.8	0.983

Table 6
Thermodynamic parameters for different pollutants removal at different temperatures.

Adsorbent	Pollutants	ΔH (kJ mol^{-1})	ΔS (J mol K^{-1})	ΔG (kJ mol^{-1})		
				303 (K)	313 (K)	323 (K)
SiO_2	AZ	−15.6	56.7	−1.07	−1.64	−2.2
	AB	−16.2	42.2	−1.16	−1.58	−2.0
	RD	−12.9	61.0	−0.94	−1.56	−2.1
	PD	−14.6	53.7	−1.05	−1.59	−2.6
ZnO@SiO_2	AZ	−16.7	60.2	−0.90	−1.5	−2.1
	AB	−13.2	48.7	−1.02	−1.5	−1.9
	RD	−14.7	55.0	−1.33	−1.88	−2.4
	PD	−11.8	44.5	−1.22	−1.66	−2.1

apparent diffusion coefficient. In general, a process is said to be diffusion-controlled, if the process rate is dependent on the diffusion rate of the two components [52]. Intra-particle diffusion model can be used to explore the possibility of intra-particle diffusion process and according to which the amount adsorbed at time t, q_t, reads;

$$q_t = k_i t^{1/2} + I \quad (8)$$

where k_i is the diffusion rate constant (mg/(g min$^{1/2}$)) and I is the intercept. If Weber–Morris plot of q_t versus $t^{1/2}$ provides a straight line, it defines intra-particle adsorption process only. Whereas, if the data shows multiple linear plots (showing influence of two or more steps) in the adsorption process, it indicates that adsorption mechanism involves more than two steps. It is assumed in the early stage of adsorption, external force plays an important role in the accumulation of adsorbate encircling the surface of the adsorbent (represented by first linear portion). Second, linear portion shows the controlled intra-particle diffusion. Fig. 8a and b shows the plots of pollutants uptake (q_t) vs. $t^{1/2}$. The data points are related by two straight lines – the first straight portion depicting macropore and mesopore diffusion and the second representing micropore diffusion [53]. The deviation of straight lines from the origin may be due to the difference in the rate of mass transfer in the initial and final stages of adsorption. Although, Pore diffusion is a fast process but this process does not contribute to control the total adsorption rate. Table 5 defines the intercept values indicating the thickness of boundary layers.

3.5. Effect of temperature

Temperature can also plays an important role/factor for adsorption of pollutants. To determine the nature of the adsorption process (endothermic or exothermic), adsorption for AZ, AB, RD and PD were done at different temperatures (303, 313, and 323 K). The increase in temperature results in a decrease of the values of $\ln(q_e/C_e)$ and also 1/T which specifies the exothermic nature of the adsorption process [54]. At different temperatures the values of $\ln(q_e/C_e)$ are treated according to Van't Hoff equation;

$$\ln\left(\frac{q_e}{C_e}\right) = \frac{-\Delta H}{RT} + \frac{\Delta S}{R} \quad (9)$$

where R is the universal gas constant (8.314 J mol^{-1} K^{-1}) and T is the absolute temperature. The slope (ΔH/R) and intercept (ΔS/R) were evaluated from the plot between $\ln(q_e/C_e)$ and 1/T as shown in Fig. 8c and d. At higher temperature, the adsorption process was also increased as toxic pollutants were adsorbed on the surface of monoliths. Table 6 shows the negative values of ΔG which confirms the spontaneity of the adsorption reactions.

3.6. Reusability

Although, reusability of monoliths endures great challenges, still by treating the saturated rock like monoliths by 1 M NaOH, moderately regenerated monoliths can be achieved. Consequently, the reusability of monoliths was investigated by performing five consecutive adsorption cycles. After each cycle removal efficiency decreases up to 5–10%. Here, for extraction of mesoporous particles, specific filtration techniques are not required because of their large size. In each cycle, pollutants were adsorbed by mesoporous SiO_2 or ZnO@SiO_2 monoliths, at room temperature for 60 min. Fig. 8e and f shows reusability of SiO_2 or ZnO@SiO_2 monoliths, after 5 consecutive cycle of adsorption.

4. Conclusions

Mesoporous silica supported metal-oxide (ZnO@SiO_2) monoliths were synthesized and showed high absorption capacity and adsorption rate for removal of toxic effluents. Synthesized solid monoliths can be straightforwardly separated from aqueous solution due to their large size (0.5 cm in diameter and 0.8 cm in length) which gave a unique advantage in the form of efficient and low-cost recovery over existing systems. Adsorption and kinetic studies at pH 4 were performed for removal of AZ, PD, AB and RD in aqueous solution in batch experiments. The Freundlich model presented is the best fit to the auxiliary data for all the pollutants. Intra-particle diffusion model defines the surface diffusion occurs at the initial stage, later followed by the pore diffusion. The adsorption is controlled by chemisorption and it is thermodynamically favorable even at warmer temperatures. In conclusion, high adsorption capacity and rapid adsorption suggested that silica supported metal-oxide (ZnO@SiO_2) monolith may be a promising adsorbent for removing several toxic pollutants from wastewater.

Conflict of interest

The authors declare that there is no conflict of interests regarding the publication of this paper.

Acknowledgement

This work is supported by BRNS-DAE, India (Grant no: 34/14/63/2014) via providing fellowship and other financial assistance. Authors are also grateful to DST-SERB (Grant no: SB/FT/CS-178/2013), DST-FIST, Thapar University and Sprint Testing Solutions-Mumbai for providing instrumental facilities.

References

[1] J. Fu, Z. Chen, M. Wang, S. Liu, J. Zhang, J. Zhang, R. Han, Q. Xu, Adsorption of methylene blue by a high-efficiency adsorbent (polydopamine microspheres): kinetics, isotherm, thermodynamics and mechanism analysis, Chem. Eng. J. 259 (2015) 53–61.

[2] E.N. El Qada, S.J. Allen, G.M. Walker, Adsorption of basic dyes from aqueous solution onto activated carbons, Chem. Eng. J. 135 (2008) 174–184.
[3] L. Zhuannian, Z. Anning, W. Guirong, Z. Xiaoguang, Adsorption behavior of methyl orange onto modified ultrafine coal powder, Chin. J. Chem. Eng. 17 (2009) 942–948.
[4] Z. Ajji, A.M. Ali, Adsorption of methyl violet and brilliant blue onto poly (vinyl alcohol) membranes grafted with N-vinyl imidazole/acrylic acid, Nucl. Instrum. Meth. Phys. Res. Sect. B: Beam Interact. Mater. Atoms. 265 (2007) 362–365.
[5] L. Ai, Y. Zhou, J. Jiang, Removal of methylene blue from aqueous solution by montmorillonite/$CoFe_2O_4$ composite with magnetic separation performance, Desalination 266 (2011) 72–77.
[6] R. Ansari, Z. Mosayebzadeh, Removal of basic dye methylene blue from aqueous solutions using sawdust and sawdust coated with polypyrrole, J. Iran. Chem. Soc. 7 (2010) 339–350.
[7] M. Hasan, A. Ahmad, B. Hameed, Adsorption of reactive dye onto cross-linked chitosan/oil palm ash composite beads, Chem. Eng. J. 136 (2008) 164–172.
[8] M. Ghaedi, H. Tavallali, M. Sharifi, S.N. Kokhdan, A. Asghari, Preparation of low cost activated carbon from Myrtus communis and pomegranate and their efficient application for removal of Congo red from aqueous solution, Spectrochim. Acta Part A, Mol. Biomol. Spectrosc. 86 (2012) 107–114.
[9] M. Ghaedi, M.N. Biyareh, S.N. Kokhdan, S. Shamsaldini, R. Sahraei, A. Daneshfar, S. Shahriyar, Comparison of the efficiency of palladium and silver nanoparticles loaded on activated carbon and zinc oxide nanorods loaded on activated carbon as new adsorbents for removal of Congo red from aqueous solution: Kinetic and isotherm study, Mater. Sci. Eng.: C 32 (2012) 725–734.
[10] M. Ghaedi, G. Negintaji, H. karimi, F. Marahel, Solid phase extraction and removal of brilliant green dye on zinc oxide nanoparticles loaded on activated carbon: new kinetic model and thermodynamic evaluation, J. Indust. Eng. Chem. 20 (2014) 1444–1452.
[11] S. Kansal, M. Singh, D. Sud, Studies on photodegradation of two commercial dyes in aqueous phase using different photocatalysts, J. Hazard. Mater. 141 (2007) 581–590.
[12] N. Modirshahla, A. Hassani, M.A. Behnajady, R. Rahbarfam, Effect of operational parameters on decolorization of Acid Yellow 23 from wastewater by UV irradiation using ZnO and ZnO/SnO_2 photocatalysts, Desalination 271 (2011) 187–192.
[13] P. Liang, L. Zhang, X. Zhao, J. Li, L. Liu, R. Cai, D. Yang, A. Umar, Synthesis of $ZnFe_2O_4/TiO_2$ composite nanofibers with enhanced photoelectrochemical activity, Sci. Adv. Mater. 7 (2015) 295–300.
[14] C. Mondal, J. Pal, M. Ganguly, A.K. Sinha, J. Jana, T. Pal, A one pot synthesis of Au–ZnO nanocomposites for plasmon-enhanced sunlight driven photocatalytic activity, New J. Chem. 38 (2014) 2999.
[15] K. Simeonidis, S. Mourdikoudis, E. Kaprara, M. Mitrakas, L. Polavarapu, Inorganic engineered nanoparticles in drinking water treatment: a critical review, Environ. Sci.: Water Res. Technol. 2 (2016) 43–70.
[16] J. Choina, A. Bagabas, C. Fischer, G.U. Flechsig, H. Kosslick, A. Alshammari, A. Schulz, The influence of the textural properties of ZnO nanoparticles on adsorption and photocatalytic remediation of water from pharmaceuticals, Catal. Today 241 (2015) 47–54.
[17] J. Liu, Z.-Y. Hu, Y. Peng, H.-W. Huang, Y. Li, M. Wu, X.-X. Ke, G.V. Tendeloo, B.-L. Su, 2D ZnO mesoporous single-crystal nanosheets with exposed 0001 polar facets for the depollution of cationic dye molecules by highly selective adsorption and photocatalytic decomposition, Appl. Catal. B: Environ. 181 (2016) 138–145.
[18] S.S. Patil, M.G. Mali, M.S. Tamboli, D.R. Patil, M.V. Kulkarni, H. Yoon, H. Kim, S.S. Al-Deyab, S.S. Yoon, S.S. Kolekar, B.B. Kale, Green approach for hierarchical nanostructured Ag-ZnO and their photocatalytic performance under sunlight, Catal. Today 260 (2016) 126–134.
[19] A.H. Lu, J.H. Smått, M. Lindén, Combined surface and volume templating of highly porous nanocast carbon monoliths, Adv. Funct. Mater. 15 (2005) 865–871.
[20] B. Tian, X. Liu, H. Yang, S. Xie, C. Yu, B. Tu, D. Zhao, General synthesis of ordered crystallized metal oxide nanoarrays replicated by microwave-digested mesoporous silica, Adv. Mater. 15 (2003) 1370–1374.
[21] K. Zhu, B. Yue, W. Zhou, H. He, Preparation of three-dimensional chromium oxide porous single crystals templated by SBA-15, Chem. Commun. (2003) 98–99.
[22] H. Yang, Q. Shi, B. Tian, Q. Lu, F. Gao, S. Xie, J. Fan, C. Yu, B. Tu, D. Zhao, One-step nanocasting synthesis of highly ordered single crystalline indium oxide nanowire arrays from mesostructured frameworks, J. Am. Chem. Soc. 125 (2003) 4724–4725.
[23] S. Laha, R. Ryoo, Synthesis of thermally stable mesoporous cerium oxide with nanocrystalline frameworks using mesoporous silica templates, Chem. Commun. (2003) 2138–2139.
[24] W. Cheng, F. Rechberger, M. Niederberger, Three-dimensional assembly of yttrium oxide nanosheets into luminescent aerogel monoliths with outstanding adsorption properties, ACS Nano 10 (2016) 2467–2475.
[25] J.H. Smått, F.M. Sayler, A.J. Grano, M.G. Bakker, Formation of hierarchically porous metal oxide and metal monoliths by nanocasting into silica monoliths, Adv. Eng. Mater. 14 (2012) 1059–1073.
[26] T. Sano, Y. Oumi, Mesoporous silica as nanoreactor for olefin polymerization, Catal. Surv. Asia 8 (2004) 295–304.
[27] P. Kannusamy, T. Sivalingam, Synthesis of porous chitosan-polyaniline/ZnO hybrid composite and application for removal of reactive orange 16 dye, Colloids Surf. B, Biointerf. 108 (2013) 229–238.
[28] M. Ghaedi, M. Ghayedi, S.N. Kokhdan, R. Sahraei, A. Daneshfar, Palladium, silver, and zinc oxide nanoparticles loaded on activated carbon as adsorbent for removal of bromophenol red from aqueous solution, J. Indust. Eng. Chem. 19 (2013) 1209–1217.
[29] J. Feng, Y. Wang, L. Zou, B. Li, X. He, Y. Ren, Y. Lv, Z. Fan, Synthesis of magnetic ZnO/ZnFe2O4 by a microwave combustion method, and its high rate of adsorption of methylene blue, J. Colloid Interf. Sci. 438 (2015) 318–322.
[30] N.K. Amin, Removal of reactive dye from aqueous solutions by adsorption onto activated carbons prepared from sugarcane bagasse pith, Desalination 223 (2008) 152–161.
[31] A. Mittal, D. Kaur, J. Mittal, Batch and bulk removal of a triarylmethane dye Fast Green FCF, from wastewater by adsorption over waste materials, J. Hazard. Mater. 163 (2009) 568–577.
[32] M. Sharma, A. Mishra, A. Mehta, D. Choudhury, S. Basu, Effect of surfactants on the structure and adsorption efficiency of hydroxyapatite nanorods, J. Nanosci. Nanotechnol. 17 (2017) 1–11.
[33] C.A. Başar, Applicability of the various adsorption models of three dyes adsorption onto activated carbon prepared waste apricot, J. Hazard. Mater. 135 (2006) 232–241.
[34] S. Chatterjee, S. Chatterjee, B.P. Chatterjee, A.K. Guha, Adsorptive removal of Congo red, a carcinogenic textile dye by chitosan hydrobeads: binding mechanism, equilibrium and kinetics, Colloids Surf. A: Physicochem. Eng. Aspects 299 (2007) 146–152.
[35] A. Shukla, Y.-H. Zhang, P. Dubey, J. Margrave, S.S. Shukla, The role of sawdust in the removal of unwanted materials from water, J. Hazard. Mater. 95 (2002) 137–152.
[36] I.D. Mall, V.C. Srivastava, N.K. Agarwal, I.M. Mishra, Removal of Congo red from aqueous solution by bagasse fly ash and activated carbon: kinetic study and equilibrium isotherm analyses, Chemosphere 61 (2005) 492–501.
[37] W.J. Thomson, Introduction to transport phenomena, Pearson College Division, 2000.
[38] A. Mittal, D. Kaur, J. Mittal, Applicability of waste materials—bottom ash and deoiled soya—as adsorbents for the removal and recovery of a hazardous dye, brilliant green, J. Colloid Interf. Sci. 326 (2008) 8–17.
[39] E. Hassan, Comparative study on the biosorption of Pb (II), Cd (II) and Zn (II) using Lemon grass (Cymbopogon citratus): kinetics, isotherms and thermodynamics, Chem. Int. 2 (2016) 89–102.
[40] R.S. Juang, F.C. Wu, R.L. Tseng, Mechanism of adsorption of dyes and phenols from water using activated carbons prepared from plum kernels, J. Colloid Interf. Sci. 227 (2000) 437–444.
[41] S. Subramani, N. Thinakaran, Isotherm, kinetic and thermodynamic studies on the adsorption behaviour of textile dyes onto chitosan, Process Safety Environ. Protect. 106 (2017) 1–10.
[42] M.J. Iqbal, M.N. Ashiq, Adsorption of dyes from aqueous solutions on activated charcoal, J. Hazard. Mater. 139 (2007) 57–66.
[43] M. Xu, Y. Zhang, Z. Zhang, Y. Shen, M. Zhao, G. Pan, Study on the adsorption of Ca^{2+}, Cd^{2+} and Pb^{2+} by magnetic Fe_3O_4 yeast treated with EDTA dianhydride, Chem. Eng. J. 168 (2011) 737–745.
[44] A.H. Chen, C.Y. Yang, C.Y. Chen, C.W. Chen, The chemically crosslinked metal-complexed chitosans for comparative adsorptions of Cu(II), Zn(II), Ni(II) and Pb (II) ions in aqueous medium, J. Hazard. Mater. 163 (2009) 1068–1075.
[45] X. Tan, X. Wang, M. Fang, C. Chen, Sorption and desorption of Th(IV) on nanoparticles of anatase studied by batch and spectroscopy methods, Colloids Surf. A: Physicochem. Eng. Aspects 296 (2007) 109–116.
[46] V.K. Gupta, B. Gupta, A. Rastogi, S. Agarwal, A. Nayak, Pesticides removal from waste water by activated carbon prepared from waste rubber tire, Water Res. 45 (2011) 4047–4055.
[47] N. Kataria, V.K. Garg, M. Jain, K. Kadirvelu, Preparation, characterization and potential use of flower shaped Zinc oxide nanoparticles (ZON) for the adsorption of Victoria Blue B dye from aqueous solution, Adv. Powder Technol. 27 (2016) 1180–1188.
[48] Z. Monsef Khoshhesab, K. Gonbadi, G. Rezaei Behbehani, Removal of reactive black 8 dye from aqueous solutions using zinc oxide nanoparticles: investigation of adsorption parameters, Desalin. Water Treat. 56 (2014) 1558–1565.
[49] M. Ghaedi, A. Hassanzadeh, S.N. Kokhdan, Multiwalled carbon nanotubes as adsorbents for the kinetic and equilibrium study of the removal of Alizarin Red S and Morin, J. Chem. Eng. Data 56 (2011) 2511–2520.
[50] S. Chaudhary, Y. Kaur, A. Umar, G.R. Chaudhary, 1-Butyl-3-methylimidazolium tetrafluoroborate functionalized ZnO nanoparticles for removal of toxic organic dyes, J. Mol. Liquids 220 (2016) 1013–1021.
[51] F.-C. Wu, R.-L. Tseng, R.-S. Juang, Initial behavior of intraparticle diffusion model used in the description of adsorption kinetics, Chem. Eng. J. 153 (2009) 1–8.
[52] G. Crini, H.N. Peindy, F. Gimbert, C. Robert, Removal of CI Basic Green 4 (Malachite Green) from aqueous solutions by adsorption using cyclodextrin-based adsorbent: kinetic and equilibrium studies, Sep. Purif. Technol. 53 (2007) 97–110.
[53] L. Fan, C. Luo, X. Li, F. Lu, H. Qiu, M. Sun, Fabrication of novel magnetic chitosan grafted with graphene oxide to enhance adsorption properties for methyl blue, J. Hazard. Mater. 215 (2012) 272–279.
[54] G.C. Panda, S.K. Das, A.K. Guha, Jute stick powder as a potential biomass for the removal of Congo red and rhodamine B from their aqueous solution, J. Hazard. Mater. 164 (2009) 374–379.